Chapter 6

Azimuthal Structure of Particle Distribution in Relativistic Nucleus-Nucleus Collisions

6.1 Introduction

It is now confirmed that the experimental data on ^{28}Si-Ag/Br interaction at 14.5A GeV contain rapid fluctuations of produced particle multiplicity in the pseudorapidity space, which goes beyond the trivial statistical noise. The most important reason of the observed fluctuation as advocated in refs. [1–3], is the Bose-Einstein Correlation (BEC) between identical bosons. Another probable reason that has recently drawn the interest of several heavy-ion research groups is the emission of Cherenkov gluons [4, 5], or the formation of Mach shock waves [6–8] within the partonic/nuclear medium. In either case the resulting wavefront bears a conical structure, which is characterized by a semi-vertex angle α given by

$$\cos\alpha = \frac{v_{\rm med}}{v} = \frac{v_0}{\mu v}. \tag{6.1}$$

Depending upon the case as it may be, $v_{\rm med} = v_0/\mu$ is either the velocity of the gluons or that of the shock wave in the nuclear/partonic medium, v_0 is the velocity of the gluons or the

velocity of the elastic wave in free space, μ is the refractive index of the medium concerned and v is the velocity of the partonic jet that triggers the Cherenkov gluon emission or the shock wave in the nuclear/partonic medium. In this formalism an impinging nucleus is treated as a bunch of confined partons, each of which is capable of emitting the Cherenkov gluons while traversing through a target medium. Under favorable circumstances if the conical structure of the Cherenkov wavefront can withstand the impact of collision, the consequence will be reflected in the azimuthal distribution of the final state particles [5, 9]. In this process if the number of emitted gluons is large, and if each of them generates a minijet, then a 'ring-like' structure of final state mesons distributed over the entire target azimuth may appear. On the other hand for a moderate number of emitted gluons, only a few jets are expected and the corresponding pattern is said to be a 'jet-like' structure. Similar azimuthal structures may also result due to the formation of nuclear shock waves as the impinging projectile nucleons travel with a speed greater than that of the elastic waves through the nuclear medium. Whatever may be the reason, the phenomenon still largely speculative in nature, and so far it is investigated without taking the BEC effect into consideration [5, 10–17].

In the recent past we have reported an analysis on the azimuthal structure of charged particles in AB collisions at 200A GeV [18]. In ref. [18] two different data sets [^{32}S-Ag/Br and ^{16}O-Ag/Br] are used and the experiment is compared merely with a random number based simulation. Jet-like structures are found in the experimental data. In the present work we present similar analyses for the ^{28}Si-Ag/Br interaction at 14.5A GeV. The analysis also encompasses ^{32}S-Ag/Br data at 200A GeV for a ready reference and systematic comparison. Following the trend of our analysis, the experiments are compared with the UrQMD. In addition to UrQMD we also consider the Relativistic Quantum Molecular Dynamics (RQMD) models [19] for comparison. In both simulations Bose-Einstein correlation is incorporated as an after burner. The simulation technique is elaborated in Section 2.5 of Chapter 2. The primary motivation of this analysis is to eliminate the known cause(s) of particle cluster formation so that any discrepancy between the experiment and the simulation can be regarded as a genuine signal of some nontrivial dynamics. For $E_{\rm lab}$ = 14.5A GeV the equivalent nucleon-nucleon (NN) center of mass energy is $\sqrt{s_{NN}}$ = 5.39 GeV and $E_{\rm lab}$ = 200A GeV corresponds to $\sqrt{s_{NN}}$ = 19.4 GeV. Thus, in our data sets the target-projectile combinations are almost of same geometrical size, but the collision energy involved ($\sqrt{s_{NN}}$) differs almost by a factor of four. We therefore, get a chance to examine the energy dependence of the effects to be investigated. The number of participating nucleons in the central collisions is more and therefore it is more likely that unnatural angular structures (if any) will be observed in central collisions.

6.2 Methodology

Without claiming any originality whatsoever, we furnish below the methodology adopted in the present analysis as elaborated in ref. [11]. Accordingly, an event with a shower track multiplicity n_s is first divided into several subgroups (or clusters) each containing a fixed number of shower tracks, say n_d. Each n_d-tuple of particles (tracks) are thereafter consecutively placed along the η-axis in increasing order of their η values. A cluster is characterized by the following quantities,

$$\text{(i)} \quad \text{a size } \Delta\eta = \eta_{\max} - \eta_{\min}, \tag{6.2a}$$

$$\text{(ii) a density } \rho = n_d/\Delta\eta, \tag{6.2b}$$

$$\text{(iii) a mean } \eta_m = \sum_{i=1}^{n_d} \eta_i/n_d. \tag{6.2c}$$

Here, $\eta_{\max}$ ($\eta_{\min}$) is the largest (smallest) η value in the particle subgroup (cluster). Since all clusters characterized by the above parameters pertain to same multiplicity n_d, they are statistically comparable with each other. For a similar analysis Gogiberidze *et al.* [20] used a different approach where instead of fixed cluster multiplicity, fixed cluster size $\Delta\eta$ was used. Two other parameters expressed in terms of the azimuthal angle φ of the shower tracks are also used to identify the jet/ring-like structures. They are,

$$S_1 = -\sum_{i=1}^{n_d} \ln(\Delta\varphi_i) \quad \text{and} \quad S_2 = \sum_{i=1}^{n_d} (\Delta\varphi_i)^2, \tag{6.3}$$

where $\Delta\varphi_i = \varphi_{i+1} - \varphi_i$ is the azimuthal gap between successive particles in the target diagram belonging to a particular cluster/subgroup, starting from the first and second, followed by second and third $\cdots$, so on, ultimately ending at the last and the first. For simplicity one can measure $\Delta\varphi_i$ in the unit of a full revolution (2π) of φ. For an ideal ring-like structure the tracks will be concentrated within a narrow η interval but isotropically distributed over the whole azimuth, while for an ideal jet-like structure the tracks will be concentrated into small dense groups within a narrow region of both η and φ. To make things clear a schematic representation of the target azimuth of an ideal ring/jet-like structure is given in Fig. 6.1. The 'S-parameters' and the cluster density ρ will decide whether the structures are ring-like or jet-like. On the other hand, the cluster mean η_m and the cluster size $\Delta\eta$ help us to identify respectively, the location and the size (a measure of correlation length) of the clusters. From the definition of the S-parameters it is clear that while S_1 is sensitive to small gaps, S_2 is sensitive to large ones. In that respect S_1 and S_2 are complementary to each other. For an ideal jet-like emission $S_1 \to \infty$ and $S_2 \to 1$, and for an ideal ring-like distribution $S_1 \to n_d \ln n_d$ and $S_2 \to 1/n_d$. For a purely stochastic emission

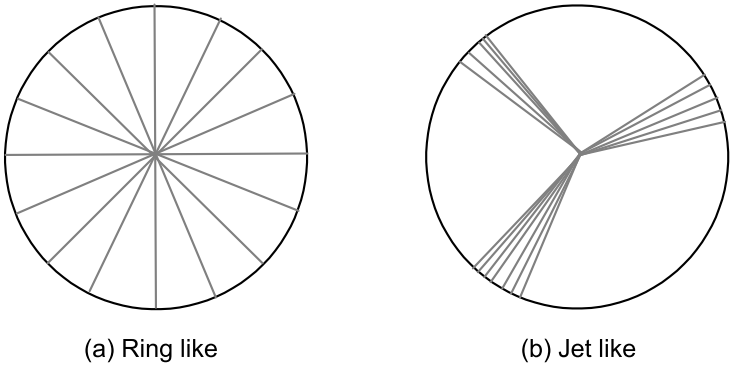

Figure 6.1: Schematic diagrams of an ideal (a) ring-like and (b) jet-like structure in the target azimuth.

of particles the $\Delta\varphi$-distribution is expected to be

$$f(\Delta\varphi) = (n_d - 1)(1 - \Delta\varphi)^{(n_d-2)}, \tag{6.4}$$

and under such a circumstance the expectation values of the S-parameters evaluated analytically are

$$\langle S_1 \rangle = n_d \sum_{k=1}^{n_d-1} \frac{1}{k} \quad \text{and} \quad \langle S_2 \rangle = \frac{2}{n_d + 1}. \tag{6.5}$$

Distributions of S_1 and S_2 parameters would be peaked around their respective stochastic expectation values. Presence of ring-like structures are reflected as an excess observed in the experiment over the respective stochastic distribution in a region left to the stochastic mean. On the other hand, for jet-like structures such excess counts would occur in a region right to the stochastic mean. A schematic of the normalized S_2 distributions of Gaussian form expected from three different processes are illustrated in Fig. 6.2. In this figure the distributions marked by 1, 2 and 3 represent, respectively the ring-like, the stochastic and the jet-like effects. The solid curve is the combined distribution of all the three individuals. Therefore, in order to extract information about the unusual azimuthal structure(s), one needs to subtract the contribution coming out of the stochastic phenomena. In this analysis the stochastic process is mimicked by using two sets of Monte-Carlo simulations, namely the RQMD and the UrQMD, both supplemented by BEC in the form of an after burner.

6.3 Results

We examine the average as well as the event-wise behavior of both S-parameters introduced above. However, in ref. [11] it is argued that to identify a jet/ring-like structure S_2 is a

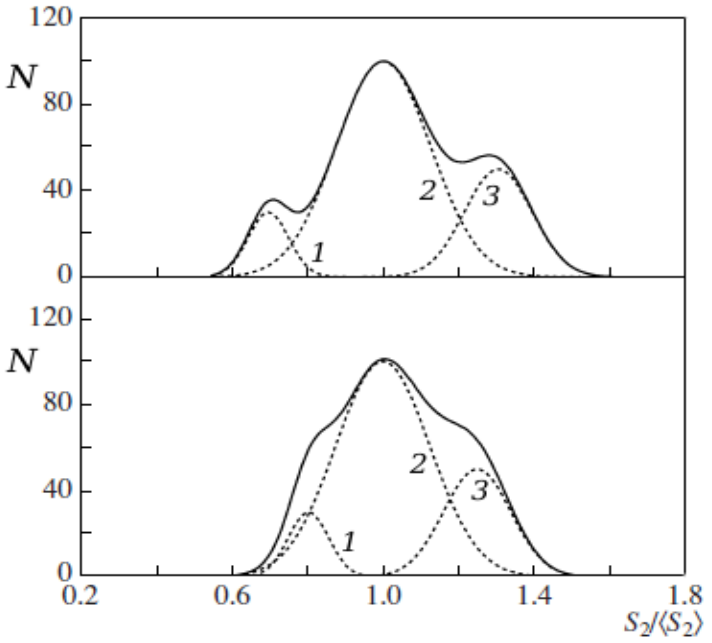

Figure 6.2: A schematic of $S_2/\langle S_2\rangle$ distributions from three effects, namely (1) ring-like effect distribution, (2) stochastic distribution and (3) jet-like effect distribution. The solid curve represents the resultant distribution.

better choice than S_1. An analysis on the cluster properties similar to that of ours, was performed by Vokál *et al.* in Pb-Ag/Br interaction at 158A GeV [16]. They found that for the high multiplicity events the effects of any unusual azimuthal structure is almost independent of the choice of the n_d value, while for the low multiplicity events such effects diminish with increasing n_d. The result of Vokál *et al.* [16] in this regard is shown in Fig. 6.3. In the present study only high multiplicity events are chosen, the multiplicity cuts taken are $n_s > 50$ for the ^{28}Si data and $n_s > 200$ for the ^{32}S data. We have checked that within the range, $10 \leqslant n_d \leqslant 25$ for the ^{28}Si-Ag/Br interaction and $25 \leqslant n_d \leqslant 50$ for the ^{32}S-Ag/Br interaction, our results depend only insignificantly on the choice of n_d. Therefore, throughout our 'ring-jet' analysis we set the subgroup multiplicity n_d to 15 for the ^{28}Si-Ag/Br interaction and to 40 for the ^{32}S-Ag/Br interaction. For this choice of the n_d values, the stochastic expectation values for the ^{28}Si-events are $\langle S_1\rangle = 48.773$ and $\langle S_2\rangle = 0.125$, while those for the ^{32}S-events are, respectively $= 170.142$ and $= 0.049$ [see Eq. (6.5)]. As a first test, we normalize the S parameters by their respective stochastic values ($\langle S_1\rangle$ and $\langle S_2\rangle$) and plot the histograms for two different AB interactions under consideration. Fig. 6.4 is drawn for the ^{28}Si-induced events, whereas Fig. 6.5 is for the ^{32}S-induced events. For comparison the corresponding RQMD+BEC and UrQMD+BEC predictions on the S-parameters are also schematically presented along with the experiment. The S-parameter distributions of ^{28}Si-Ag/Br interaction are slightly right skewed with respect to the corresponding stochastic mean values. As expected we find that the RQMD+BEC and the UrQMD+BEC

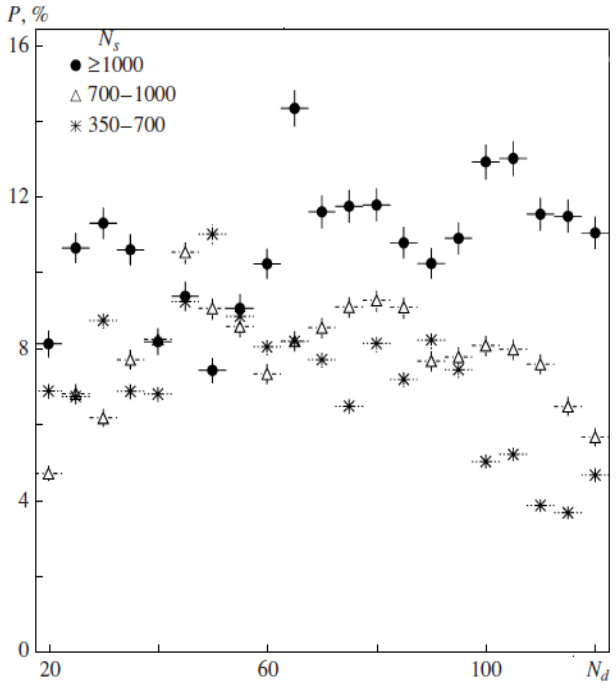

Figure 6.3: Contribution of the ring-like effect to the experimental data on ^{208}Pb-Ag/Br interaction at 158A GeV/c as a function of the number of particles in a subgroup (N_d) for three different multiplicity groups [16].

distributions are marginally different from their experimental counterparts. In each case the difference between the experiment and the simulation is shown in the respective diagram with the help of shaded histograms drawn around the S-axis. We notice that in both cases there exist small experimental excesses in the left to the stochastic mean, i.e., to the jet side. In comparison with experiment the differences are larger in RQMD+BEC simulation. For the ^{32}S-Ag/Br interaction the S-distributions once again are right skewed. The skewness however, is less in this case than the ^{28}Si-Ag/Br interaction. For ^{32}S-Ag/Br interaction the difference between experiment and simulation, once again shown by shaded histograms, lack any definite pattern and their magnitudes are smaller than the ^{28}Si-Ag/Br case. Beyond statistical uncertainties such differences are of little significance. It is to be remembered that an experimental excess in $S_i/\langle S_i\rangle < 1\ (>1):\ i = 1, 2$ region indicates ring (jet) like structures. Based on the S-parameter distributions we can therefore, say that in the ^{32}S-Ag/Br data there is hardly any indication of an unusual structure, whereas in ^{28}Si-Ag/Br data there is a small signal of ring-like structures. In a similar analysis of the Pb+Ag/Br data at 158A GeV and Au-Ag/Br data at 11.6A GeV [16, 17], experimental excesses over their respective FRITIOF model [21] predictions were obtained in the S_2-distributions on either side of $S_2/\langle S_2\rangle = 1$. It is to be remembered that for overlapping η-intervals strong correlations between particles belonging to different sub-groups will be present, and this will certainly influence the statistical errors. One way to estimate the statistical uncertainties

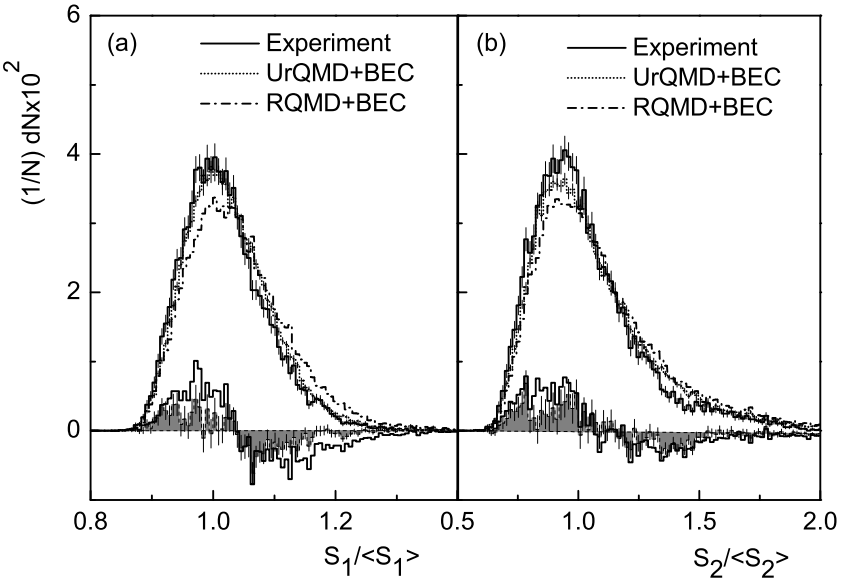

Figure 6.4: Distributions of (a) the S_1 and (b) the S_2 parameters normalized by their respective stochastic values in ^{28}Si-Ag/Br interaction at 14.5A GeV.

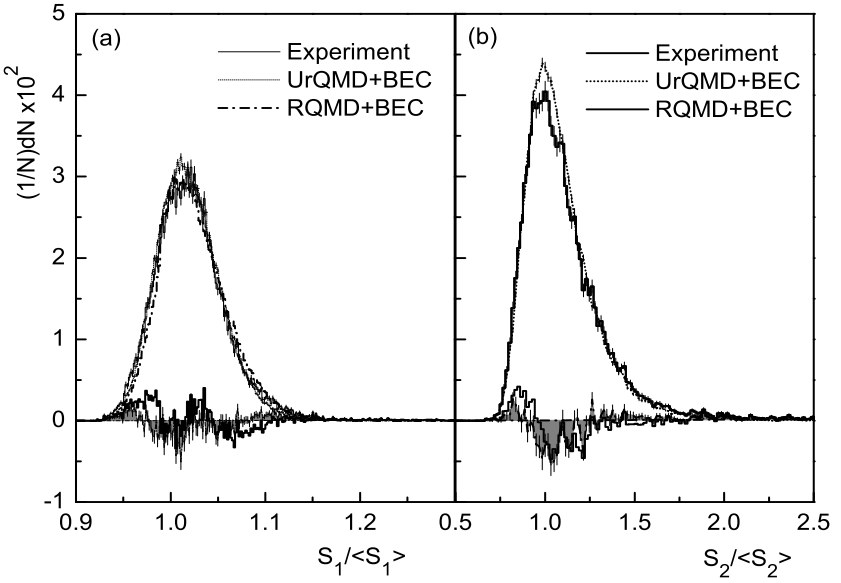

Figure 6.5: Same as Fig. 6.4 but in ^{32}S-Ag/Br interaction at 200A GeV.

in such cases is to generate several independent sets of data based on random numbers that are similar in size, multiplicity, η and φ distributions as the experiment. One can then determine the dispersion or the standard deviation of the parameter/quantity under consideration over the number of generated data sets. The statistical errors obtained in this way can be made free from the influence of such correlations. It may also be mentioned that the problem of γ-conversion and the resulting e^+e^- tracks getting mixed up with the pion tracks can influence our observation. However, this effect is more acute in vertically exposed emulsion chambers. In horizontally exposed emulsion experiments such as the present one,

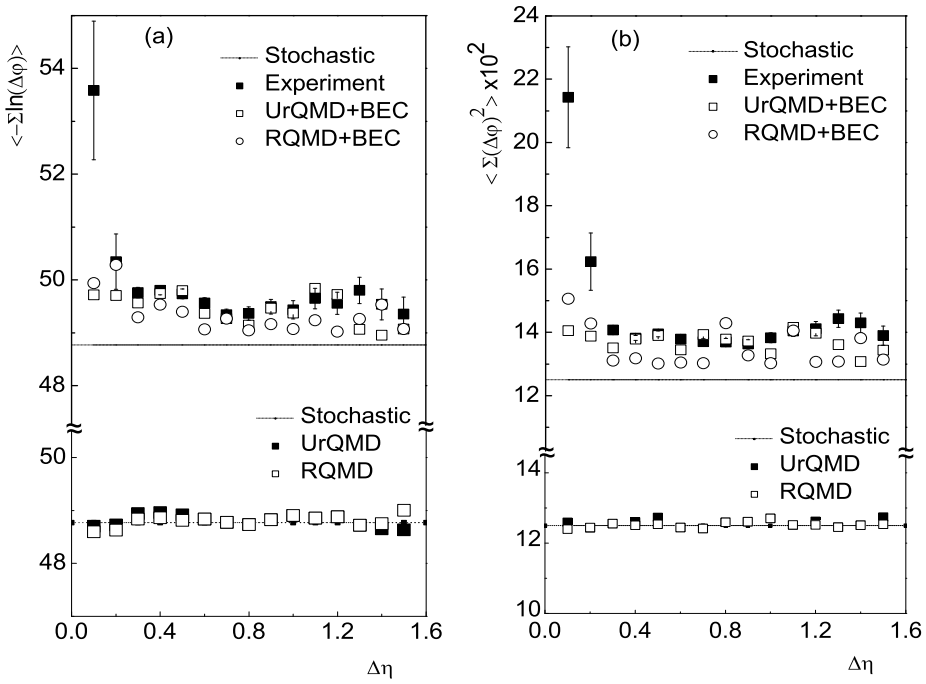

Figure 6.6: Average behavior of (a) the S_1 parameter and (b) the S_2 parameter in ^{28}Si-Ag/Br interaction at 14.5A GeV. Horizontal dashed lines follow Eq. (6.5). The effect of the BEC algorithm is shown in the bottom panel.

it is possible to follow every track back to its production point. Hence the e^+e^- pairs arising out of γ-conversion (if there is any) can easily be traced back to their point of origin which will certainly be different from the primary interaction vertex. Moreover, production of direct gamma is less in the energy range considered. The contamination by e^+e^- pairs is therefore, insignificant in the present investigation.

Following ref. [11] we also study the average behavior of the S-parameters over a small η-interval ($\Delta\eta$). The average values are given by,

$$\overline{S}_1 = \left\langle -\sum \ln(\Delta\varphi_i) \right\rangle \quad \text{and} \quad \overline{S}_2 = \left\langle \sum (\Delta\varphi_i)^2 \right\rangle, \tag{6.6}$$

where $\langle \cdots \rangle$ indicates event averaging. These average values are graphically presented as functions of $\Delta\eta$ in Fig. 6.6 and Fig. 6.7, respectively, for the ^{28}Si-Ag/Br and ^{32}S-Ag/Br events. In both figures panel (a) represents $\overline{S}_1$ while panel (b) represents $\overline{S}_2$. In each diagram the dashed lines correspond to the respective stochastic averages obtained from Eq. (6.5). The RQMD+BEC and UrQMD+BEC predictions are also incorporated in these diagrams. From these figures it is seen that the RQMD+BEC and UrQMD+BEC predictions are systematically but consistently a little above the corresponding stochastic line, indicating a positive effect of incorporating BEC into the code. If we do not incorporate BEC then both the RQMD and the UrQMD points overlap with the stochastic lines. This feature is graphically shown at the bottom of each of the diagrams (Fig. 6.6 and Fig. 6.7), indicating thereby

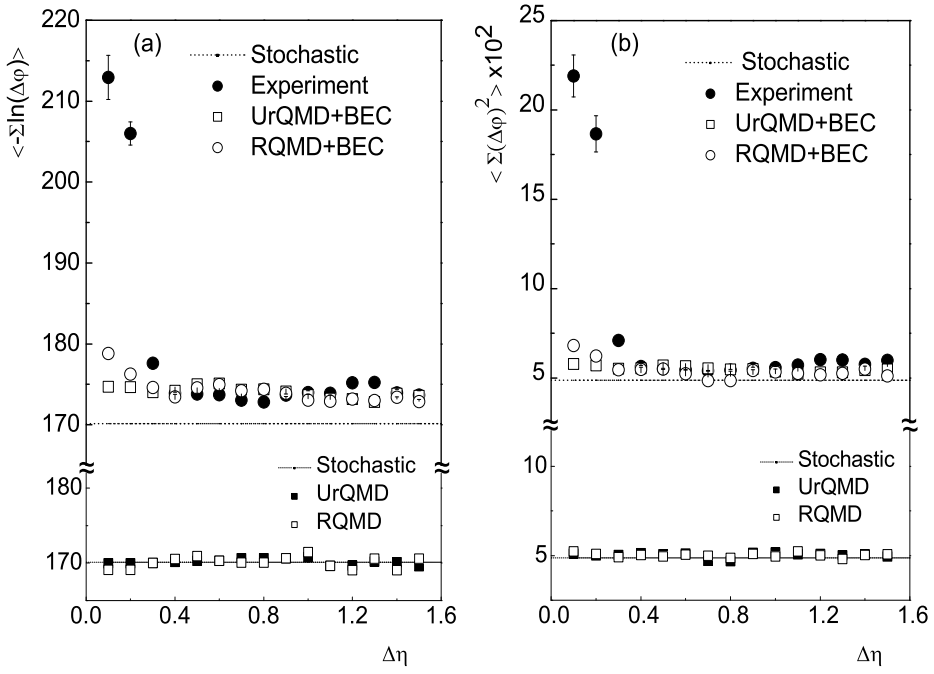

Figure 6.7: Same as Fig. 6.6 but in ^{32}S-Ag/Br interaction at 200A GeV.

absence of any correlation whatsoever among the emitted mesons. The important aspect of these diagrams is that the first one or two experimental points (up to $\Delta\eta \approx 0.2 - 0.3$) are significantly way above all the other values, and beyond $\Delta\eta \approx 0.2 - 0.3$ the experiments are always very close to the respective simulated values. In the ^{32}S-Ag/Br interaction the simulated results beyond $\Delta\eta \approx 0.3$ are almost always overlapping with each other, and both are closer to the stochastic line than what they are in the ^{28}Si-Ag/Br case. The first two or three experimental points (up to $\Delta\eta \approx 0.2 - 0.3$) also show significant deviation from the RQMD, RQMD+BEC, UrQMD, UrQMD+BEC, and the stochastic prediction. The observation confirms that short range particle correlations other than the Bose-Einstein type, are present in both the experiments. We further examine whether the contributions to the experimental excesses in the average S values within a small $\Delta\eta$ ($\approx 0.1 - 0.3$), are coming from a small η region or they are distributed over the entire η space under consideration. For this purpose the average S- parameters are now plotted as functions of both $\Delta\eta$ and η_m. Only the experimental distributions are shown in Fig. 6.8 and Fig. 6.9, respectively, for the ^{28}Si-Ag/Br and ^{32}S-Ag/Br interactions. To our surprise, we notice that while the average S_1 values are more or less uniformly distributed over a wide η range, there are very prominent peaks in the average S_2 distributions. The peaks are located within $1.0 \leqslant \eta_m \leqslant 2.0$ in the ^{28}Si-Ag/Br case and within $3.0 \leqslant \eta_m \leqslant 4.0$ in the ^{32}S-Ag/Br one. Both sets of data behave similarly, and the peaks in both cases are more or less located around the central particle producing regions. Whatever may be the reason, the results suggest that to detect any unusual structure, S_2 is indeed a better parameter than S_1 [11]. In Fig. 6.10 we

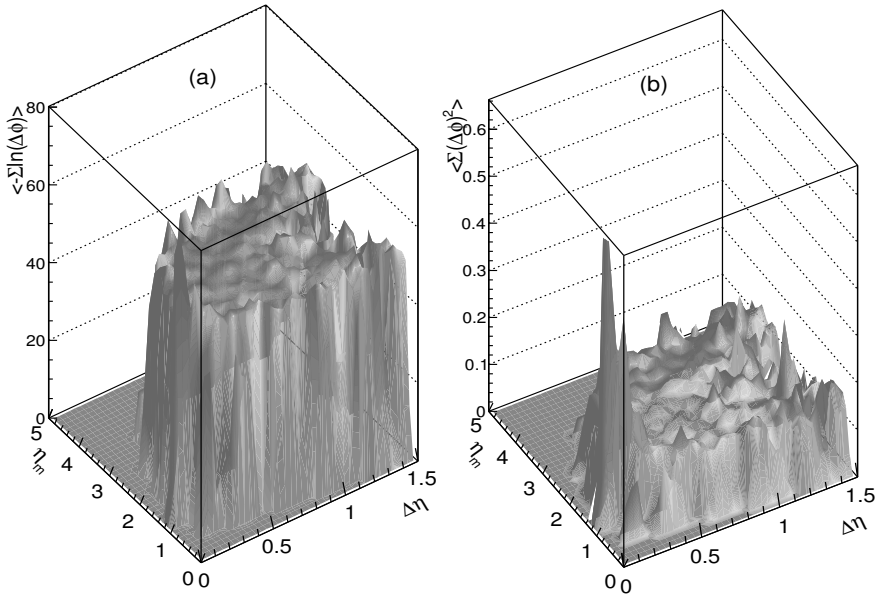

Figure 6.8: Plot of (a) $\langle -\sum \ln(\Delta\varphi)\rangle$ and (b) $\left\langle \sum(\Delta\varphi)^2 \right\rangle$ as a function of $\Delta\eta$ and η_m in ^{28}Si-Ag/Br interaction at 14.5A GeV.

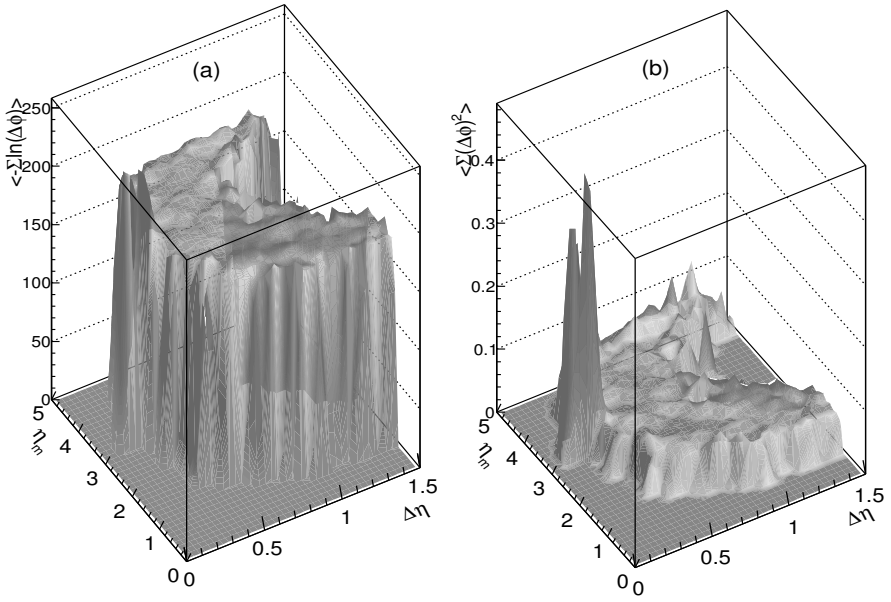

Figure 6.9: Same as Fig. 6.8 but in ^{32}S-Ag/Br interaction at 200A GeV.

plot the cluster density distributions for the ^{28}Si-Ag/Br events, like before for the experiment as well as for the simulated data. Fig. 6.10(a) represents the regions which should be dominated by the ring-like structure, $S_2/\langle S_2\rangle < 1$, and Fig. 6.10(b) represents the regions which should be dominated by the jet-like structures, $S_2/\langle S_2\rangle > 1$. Similar plots for the ^{32}S-Ag/Br events are shown in Fig. 6.11. While both the ^{28}Si-Ag/Br diagrams are slightly

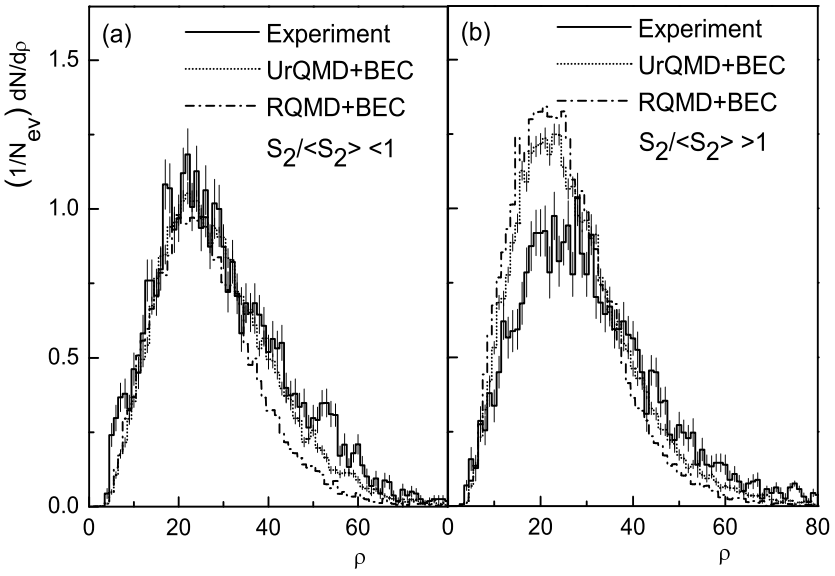

Figure 6.10: Cluster density distributions for (a) the ring-like region, $S_2/\langle S_2\rangle < 1$ and (b) the jet-like region, $S_2/\langle S_2\rangle > 1$ in ^{28}Si-Ag/Br interaction at 14.5A GeV.

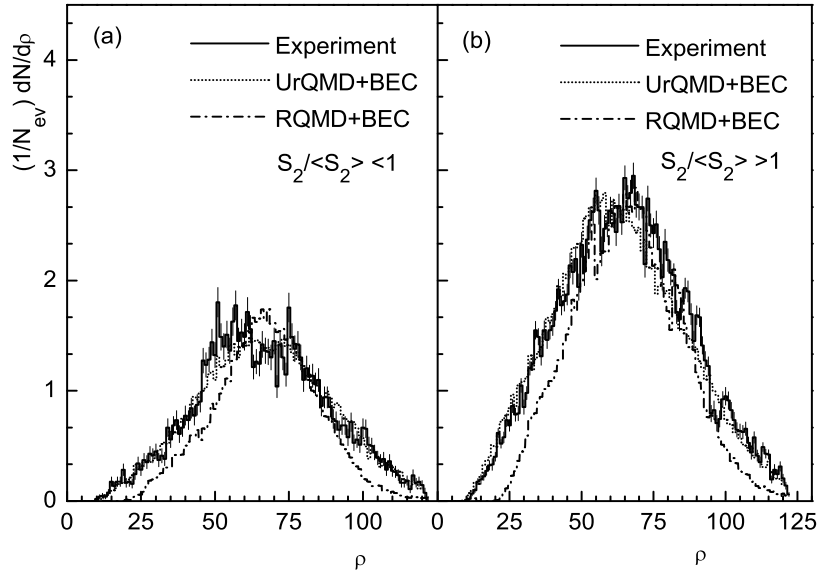

Figure 6.11: Same as Fig. 6.10 but in ^{32}S-Ag/Br interaction at 200A GeV.

right skewed, the ^{32}S-Ag/Br diagrams are more symmetric. If dense groups of particles are present in these data samples, then an excess experimental count over the background noise should have appeared. Occasional differences between the experiment and the simulation are seen in all diagrams. In Fig. 6.10(a) these differences are statistically not very significant. Even in Fig. 6.11(a) the experimental excesses over the simulation are not too large. Differences between experiment and RQMD+BEC are more than those between the

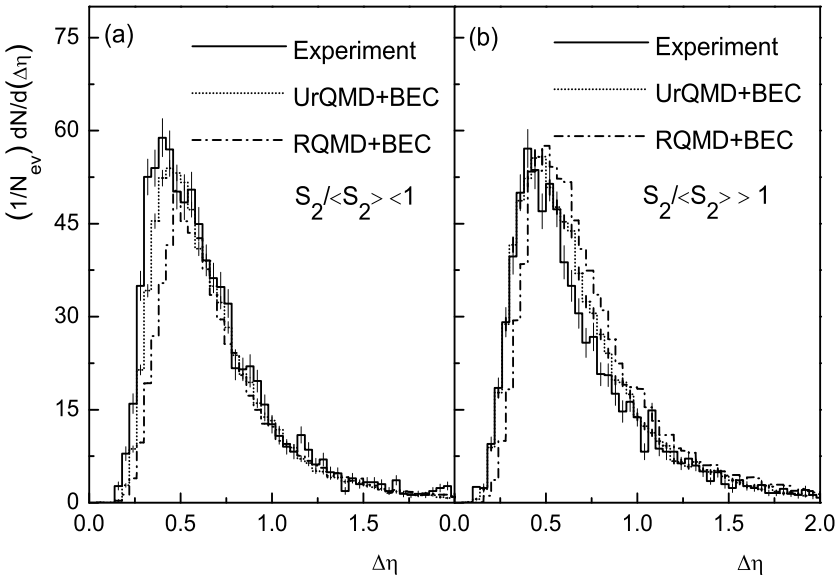

Figure 6.12: Cluster size distributions for (a) the ring-like region, $S_2/\langle S_2\rangle < 1$ and (b) the jet-like region, $S_2/\langle S_2\rangle > 1$ in ^{28}Si-Ag/Br interaction at 14.5A GeV.

experiment and the UrQMD+BEC. The results are consistent with our previous observations [18]. To have an idea about the cluster size, we plot the $\Delta\eta$ distributions in Fig. 6.12 and Fig. 6.13, respectively, for the ^{28}Si-Ag/Br and the ^{32}S-Ag/Br data samples. As usual, separate graphs are plotted for regions that should be dominated by the ring-like and the jet-like structures. We notice that all these distributions are asymmetric (right skewed). In the ^{28}Si-induced experiment significant excesses over the simulation are seen in the region that should be dominated by ring-like structures ($S_2/\langle S_2\rangle < 1$) particularly in the left to the peak (small $\Delta\eta < 0.5$) of the distribution. For $S_2/\langle S_2\rangle > 1$ the experiment is either well reproduced or the UrQMD+BEC simulation exceeds the experiment. In ^{32}S-Ag/Br events a very narrow and sharp experimental excess is observed in the distribution at $\Delta\eta \approx 0.5$ for $S_2/\langle S_2\rangle < 1$. While in the probable jet-like region ($S_2/\langle S_2\rangle > 1$) there is a broader and significant experimental excess over the simulation in and around the peak of the distribution ($0.5 \leqslant \Delta\eta \leqslant 0.7$). Barring a very narrow and sharp structure around $\Delta\eta \approx 0.5$ observed in Fig. 6.12(a), all other observations are consistent with our previous results which are, (i) mild effects due to ring-like structure in the ^{28}Si-Ag/Br interaction at 14.5A GeV, (ii) effects due to jet-like structures in ^{32}S-Ag/Br interaction at 200A GeV, and (iii) differences between the experiment and RQMD+BEC are consistently larger than those between the experiment and the UrQMD+BEC. The cluster position on the η-axis is investigated by plotting the η_m-distributions. For the ^{28}Si-Ag/Br interaction, these distributions are shown in Fig. 6.14, and similar plots for the ^{32}S-Ag/Br interactions are given in Fig. 6.15. The experimental distributions are more or less consistently symmetric about a mean value $\eta_m \approx 2$

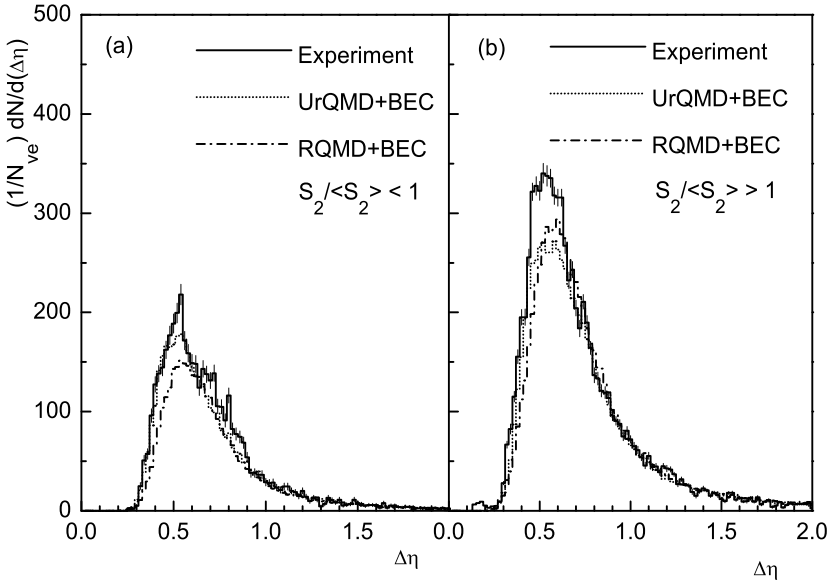

Figure 6.13: Same as Fig. 6.12 but in ^{32}S-Ag/Br interaction at 200A GeV.

for the ^{28}Si-Ag/Br events and about $\eta_m \approx 3.25$ for the ^{32}S-Ag/Br events. To separate azimuthal structure(s) originating due to different reasons, following ref. [16] we use a little more stringent conditions e.g., (i) $S_2/\langle S_2\rangle < 0.9$ due only to the ring-like structures, (ii) $0.9 < S_2/\langle S_2\rangle < 1.1$ due to the statistical effects, and (iii) $S_2/\langle S_2\rangle > 1.1$ due only to the jet-like structures. For ^{28}Si-Ag/Br events we see that (i) in the η_m-distribution the region that should be dominated by ring-like structures ($S_2/\langle S_2\rangle < 0.9$) at a couple of places e.g., at $\eta_m \approx 1.5$ and 2.2, the experiment significantly exceeds the UrQMD+BEC simulation. For $0.9 < S_2/\langle S_2\rangle < 1.1$ the experiment and the simulation more or less match each other within statistical uncertainties. On the other hand, for $S_2/\langle S_2\rangle > 1.1$ except at the extreme right hand side tail ($\eta_m > 3.6$) the simulation either matches or dominates over the corresponding experimental values. For the ^{32}S-Ag/Br interaction in $S_2/\langle S_2\rangle < 0.9$ region small experiment-simulation mismatch can be seen at several places. They are however, statistically not very significant. In the $0.9 < S_2/\langle S_2\rangle < 1.1$ region there are experimental excesses over the simulation in the central η_m-region, the reason of which may probably be attributed to the limited statistics of the experiment. In the $S_2/\langle S_2\rangle > 1.1$ region there are however significant experimental surplus over the simulation at several places, which indicate presence of jet-like structures at different η_m-locations. We notice that in this case also the RQMD+BEC results either underestimate the experiment, or they behave similarly as the UrQMD+BEC results.

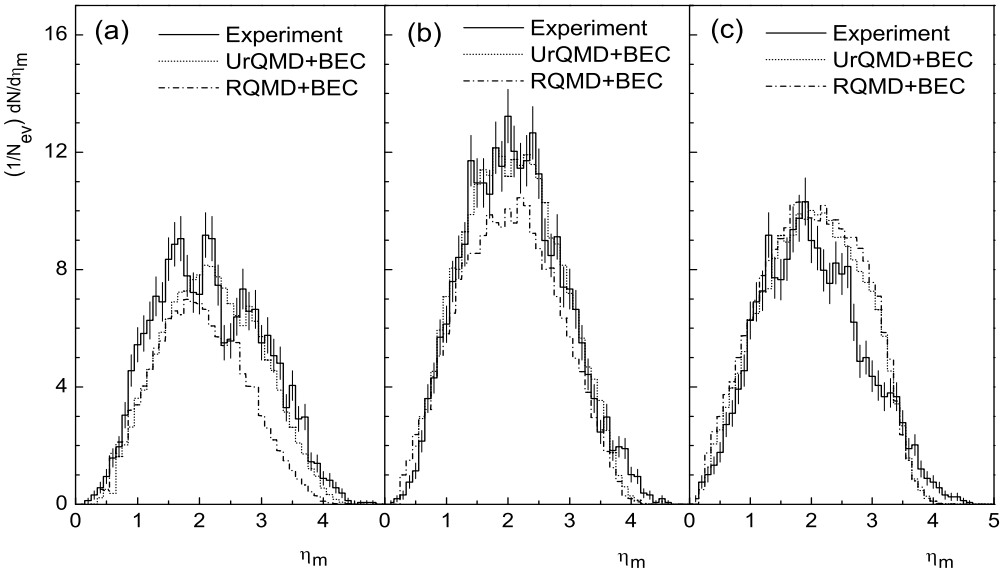

Figure 6.14: Cluster mean η_m distributions for (a) $S_2/\langle S_2\rangle < 0.9$, (b) $0.9 < S_2/\langle S_2\rangle > 1.1$ and (c) $S_2/\langle S_2\rangle > 1.1$ in ^{28}Si-Ag/Br interaction at 14.5A GeV.

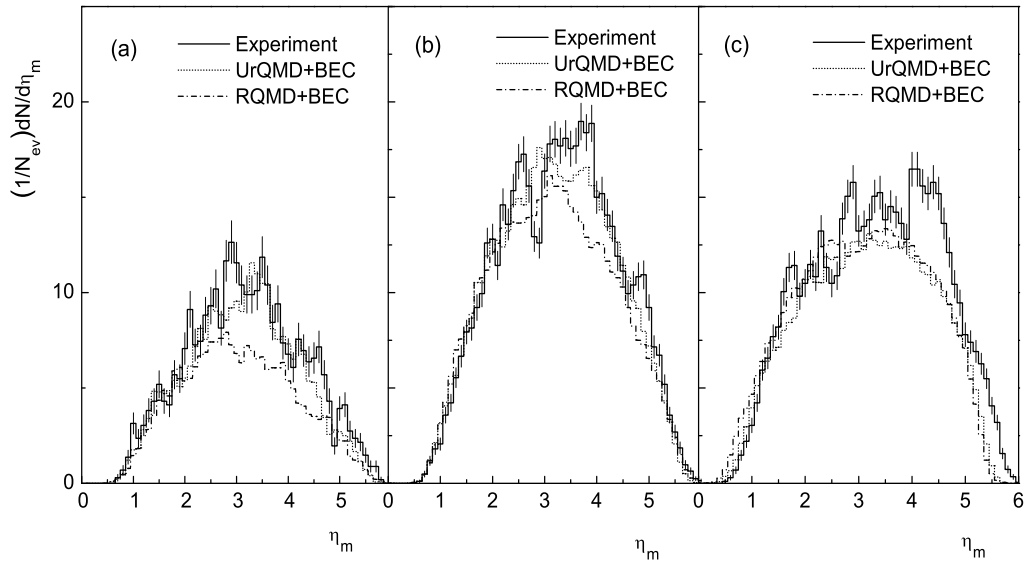

Figure 6.15: Same as Fig. 6.14 but in ^{32}S-Ag/Br interaction at 200A GeV.

6.4 Discussion

The azimuthal substructures of shower track emission from ^{28}Si-Ag/Br interaction at 14.5A GeV and from ^{32}S-Ag/Br interaction at 200A GeV are investigated under the framework of the Cherenkov gluon emission and/or the Mach shock wave formation. The experimental results are compared with the RQMD and the UrQMD models where the Bose-Einstein correlation effect has also been taken into account as an after burner. In general we find

that there are occasional but statistically significant differences between the experiment and the simulation. In comparison with the experiment, the RQMD model differs more than the UrQMD. A brief discussion on our results obtained from the present analysis is given below.

We conjecture that at $E_{\rm lab} \sim 10^1 - 10^2$ GeV/nucleon, the probability of formation of ring and/or jet-like clusters is small. At this energy scale the phenomenon is not very much energy dependent, rather it depends more on the colliding objects [11, 16–18]. In ^{28}Si-Ag/Br interaction at 14.5A GeV an indication of, however small it may be, ring-like structure is observed. The feature may be attributed to the comparatively lower incident energy, where the conical structure if formed during the initial stage of the collision, has probably survived the impact of collision. On the contrary in ^{32}S-Ag/Br interaction at 200A GeV there are indications of augmentation of jet-like structures, which is not very unusual. From our analysis we can at least claim that, whatever may be the reason (nuclear or partonic) behind the signals that we see in our experiments, they are beyond any known dynamics such as the Bose-Einstein correlation. In particular the prominent short range structures in the average S parameter values that we find in the central particle producing region (Fig. 6.8 and 6.9), are certainly due to some nontrivial reasons. With all probability at incident energies $E_{\rm lab} \sim 10 - 200$A GeV nuclear phenomenon like formation of Mach shock waves, rather than partonic effects (e.g., Cherenkov gluon emission) dominates. In our ^{28}Si-Ag/Br data we see small peaks at certain η_m values in the ring-like region ($\eta_m \approx 1.5$ and 2.2). Similarly in the ^{32}S-Ag/Br data significant excesses in the η_m distribution are seen in the jet region, at $\eta_m \approx 3.0$ and 4.5. With the knowledge of the velocity distribution of the nucleon/partonic jet in the nuclear/partonic medium, it would be a worthwhile exercise to estimate the speed of sound wave/refractive index in nuclear/partonic matter, either of which can serve significant purpose to constrain the nuclear equations of state.

Bibliography

[1] P. Carruthers *et al.*, *Phys. Lett.* **B 222**, 487 (1989).

[2] K. Kadiza and P. Seyboth, *Phys. Lett.* **B 287**, 363 (1992).

[3] M. Gyulassy and L. van Hove, in *Multiparticle Dynamics*, Eds. A. Giovannini and W. Kittel (World Scientific, Singapore, 1990).

[4] I. M. Dremin, *Pis'ma Zh. Eksp. Teor. Fiz.* **30**, 152 (1979) [*JETP Lett.* **30**, 140 (1979)].

[5] I. M. Dremin, *Yad. Fiz.* **33**, 1357 (1981) [*Sov. J. Nucl. Phys.* **33**, 726 (1981)].

[6] J. Hofmann *et al., Phys. Rev. Lett.* **36**, 88 (1976).

[7] A. E. Glassgold, W. Heckrotte, and K. M. Watson, *Ann. Phys.* **6**, 1 (1959).

[8] J. G. Ulery, *J. Phys.* **G 35**, 104032 (2008).

[9] I. M. Dremin, *Pis'ma Zh. Eksp. Teor. Fiz.* **34**, 594 (1981).

[10] A. B. Apanasenko *et al., Pis'ma Zh. Eksp. Teor. Fiz.* **30**, 157 (1979) [*JETP Lett.* **30**, 145 (1979)].

[11] M. I. Adamovich *et al.* (EMU01 Collaboration), *J. Phys.* **G 19**, 2035 (1993).

[12] A. El-Naghy and K. S. Abdel-Khalek, *Phys. Lett.* **B 299**, 370 (1993).

[13] N. M. Agababyan *et al.* (NA22 Collaboration), *Phys. Lett.* **B 389**, 397 (1996).

[14] S. Wang *et al.*, *Phys. Lett.* **B 427**, 385 (1998).

[15] I. M. Dremin *et al.*, *Phys. Lett.* **B 499**, 97 (2001).

[16] S. Vokál *et al., Proceedings of the Hadronic Structure* (Slovakia, 2004);
S. Vokál *et al., Phys. Atom. Nucl.* **71**, 1395 (2008).

[17] S. Vokál, G. I. Orlova, and S. Lehocká, *Phys. Atom. Nucl.* **72**, 237 (2009).

[18] M. K. Ghosh *et al.*, *Nucl. Phys.* **A 858**, 67 (2011).

[19] H. Sorge, *Phys. Rev.* **C 52**, 3291 (1995);
H. Sorge *et al., Ann. Phys.* **192**, 266 (1989); *Nucl. Phys.* **A 498**, 567c (1989).

[20] G. L. Gogiberidze *et al., Phys. Atom. Nucl.* **64**, 143 (2001);
G. L. Gogiberidze, E. K. Sarkisyan, and L. K. Gelovani, *Nucl. Phys.*, **B 92**, 75 (2001).

[21] B. Nilsson-Almqvist and E. Stenlund, *Comp. Phys. Commun.* **43**, 387 (1987).